CHAPTER IV
EQUILIBRIUM, KINETICS, AND MECHANISM OF LEAD ADSORPTION USING NANO ZERO-VALENT IRON COATED ON DIATOMITE

Nano zero-valent iron coated on diatomite (nZVI-D) was investigated for Pb^{2+} removal from water. It was synthesized by impregnating the diatomite with ferric sulphate, followed by chemical reduction with $NaHB_4$. In this study, nZVI-D was used to investigate the removal of Pb^{2+} in the concentration range of 100-1,250 mg/L. The adsorption isotherms well fitted using a langmuir adsorption isotherm, indicating the adsorption process to be chemisorption. The maximum adsorption capacity was found to be 158.73 mg/g at 30ºC. The intraparticle diffusion model described that the intraparticle diffusion was the rate-limiting step. The kinetics adsorption data could be well described by pseudo-second-order model. The overall of thermodynamic parameters adsorption process was endothermic and spontaneous in nature. An adsorption mechanism was proposed by using XPS data. Three steps of the adsorption were suggested, (i) Pb^{2+} ions were oxidized to Pb^0 on nZVI active sites, (ii) ferrous ions reacted with the Pb^{2+} to form FeOPbOH, PbO-Fe, PbO_2-Fe_2O_3, and PbO-FeOOH species on nZVI surface, and (iii) Pb^{2+} turned to PbO_2-Si, PbO-Si, $Pb(OH)_2$-Al, and PbO_2-Al_2O_3 on diatomite surface.

4.1 Introduction

An increasing levels of toxic heavy metals have been discharged into the environment as industrial wastes caused a severe threat to human health, and ecological systems (Schmitt, Brumbaugh, & May, 2007; Zhang, Lin, Lu, & Chen, 2010). Lead is one of the most widespread pollutants in the environment. It can cause anemia, nervous system disorders, and reproductive system, liver and kidney diseases, and peripheral nervous systems (Dou & Zhang, 2011). Therefore, World Health

This paper is accepted to publish in journal Desalination and Water Treatment.

Organization (WHO) has set a drinking-water standard for lead concentration of less than 0.01 mg/L (WHO, 2012). Ion exchange, filtration, chemical precipitation, and adsorption are used to remove heavy metals from wastewaters (Bessbousse, Rhlalou, Verchère, & Lebrun, 2008; Chao & Chang, 2012; Feng, Lin, Gong, Sugita, & Shoya, 2004; Naeem, Saddique, Mustafa, Kim, & Dilara, 2009). Among these methods, adsorption is a highly competent and economical removal technique. It has low toxicity, strong reducing agent and the metal is the most suitable for using in the environment (Kundu & Gupta, 2007; Mak, Rao, & Lo, 2011).

Nanoscale zero-valent iron (nZVI) has been widely used for an in-situ remediation of ground water and surface water as a suitable donor of electrons. A redox couple of Fe^0 and dissolved Fe^{2+} form has a standard reduction potential of 0.447 V (Ponder et al., 2001.). Thus, it can be used as an adsorbent for heavy metal. It has also been confirmed that nZVI can remove metalloid and metallic contaminants (Li, Elliott, & Zhang, 2006). In spite of the above-mentioned advantages of nZVI, in many cases nanoparticles agglomerate due to Van der Waals and magnetic attraction forces which may lead to the loss of the benefits associated with their natural high specific surface area. For this reason, the stabilization of nZVI on a support with a good dispersion can lead to steady or enhance the remediation capability. The dispersion of nZVI on the support improves the adsorption capacity through preventing agglomeration of iron nanoparticles and exposing highly reactive nanoparticles directly to the contaminants. The support materials, activated carbon, zeolite, bentonite, pillared clay, sand, and diatomite (Dou, Li, Zhao, & Liang, 2010; Kim et al., 2013; Mak et al., 2011; Pan, Chiou, & Lin, 2010; Zhang, Li, Li, Hu, & Zheng, 2011) are widely used. It has been reported that the porous structure of the matrix provide high hydraulic conductivity which can yield a faster heavy metals removal rates (Kim et al., 2013; Mak et al., 2011). Among the supports, synthesized zeolite showed a good adsorption performance, however, it had disadvantages due to the cost of preparation was very high. Since, diatomite ($SiO_2 \cdot nH_2O$) is a kind of natural zeolite, soft and lightweight with porous structure. It provides many unique properties, such as high porosity (80-90% voids), high surface area and chemical inertness and it is widely used as filter agents, catalyst carriers, building materials and wastewater treatment agents (organic and inorganic) (Köseoglu, Köksal, Çiftci, &

Akkurt, 2005; Pan et al., 2010; Sheng et al., 2009). Thus, it becomes an interesting material to use as a support for nZVI. Generally, supported nZVI adsorbent has to be used immediately after preparation due to it can be oxidized rapidly. In this work, coating process has been chosen to stabilize a zero-valent iron on diatomite surface. Moreover, nano zero-valent iron coated on diatomite (nZVI-D) has not been used for removing of Pb^{2+} ions from wastewater. At the same time, the understanding on mechanisms responsible for the elevation is still lacking due to the complexity of this mechanism supported nZVI system. Therefore, this research will study the mechanism of the nZVI-D by using an understanding of kinetic adsorption isotherms and adsorption isotherm.

4.2 Objectives

In this chapter will focus on (i) study of the kinetic adsorption isotherms, adsorption isotherm models, and thermodynamic, and (ii) propose mechanism of lead adsorption by nZVI-D. The results of this study can be used to evaluate the benefit of nZVI-D for heavy-metal removal, in particular lead adsorption, at the field scale.

4.3 Materials and methods

4.3.1 Materials

The sample of diatomite was achieved from the North of Thailand. Diatomite is mainly consists of SiO_2 (79.76%), Al_2O_3 (9.61%) and Fe_2O_3 (2.49%) with a specific surface area of 26.8 m^2/g. To clean up, the diatomite was washed with distilled water several times to remove the contaminants and dried at 110°C in a drying oven for 24 h, and then it was kept in the polyethylene bags. All chemicals used in all the experiments were analytical-grade reagents; namely, lead (II) nitrate ($Pb(NO_3)_2$, Ajax Finechem; Australia), iron(III) sulphate ($FeSO_4 \cdot 7H_2O$, Ajax Finechem; Australia), sodium borohydride ($NaBH_4$, Rankem; India), ammonium hydroxide (NH_4OH, Panreac; Barcelona) and hydrogen chloride (HCl_2, RCL Labscan; Thailand), together with distilled water which was purified with a illipore Milli-Q equipment (resistivity of 18 MV cm) was used in all the experiments.

4.3.2 Batch experiments for adsorption of lead by nZVI-D

As a stock solution of Pb^{2+}, the solution of 5,000 mg/L was prepared by dissolving 8 g of lead (II) nitrate ($Pb(NO_3)_2$) into distilled water and then diluted to 1,000 mL. The adsorption experiments were carried out by 500 mL of a 100 mg/L lead from stock solution with 1 g of the nZVI-D_N, and the pH was carefully adjusted of 5 (Eren, 2009; Kim et al., 2013; Momčilović, Purenović, Bojić, Zarubica, & Ranđelović, 2011; Zhang et al., 2010) by adding a small amount of diluted HCl or NH_4OH solution. The lead solutions were stirred using a mechanical magnetic stirrer with the speed of 160 rpm for 120 min.

Adsorption isotherms were obtained by varying the initial lead-ion concentrations from 250 to 1,250 mg/L in 250 mL vials with 0.5 g/L of the nZVI-D, and the pH was adjusted to 5. The experiments were conducted at room temperature. The samples were collected at 1 to 120 min. The suspensions were filtered with syringe Filter Nylon 0.45-μm membrane (Lubitech, Thailand), and the pH was adjusted to acid range to prevent the precipitation of heavy metals in solution. The difference between the initial and the final lead concentrations of the suspension was caught as the amount of lead adsorbed with atomic absorption spectroscopy (AAS, AAnalyst, Perkin Elmer, USA). The percentage removal of Pb^{2+} was defined using the following equation:

$$Y = \frac{C_0 - C_t}{C_0} \times 100 \tag{2.20}$$

where C_0 is the initial concentration of Pb^{2+} (mg/L) and C_t is the concentration of Pb^{2+} (mg/L) after adsorption at time. Y is the percentage Pb^{2+} removal.

The adsorption capacity, q_e (mg/g), was determined as follows:

$$q_e = \frac{(C_0 - C_e)}{M} V \tag{4.1}$$

where C_o and C_e are the initial and equilibrium adsorbate solution concentrations (mg/L), respectively; V is the volume of the solution (L); and M is mass of adsorbent (g).

4.4 Results and discussion

4.4.1 Adsorption efficiency of lead by diatomite, nZVI and nZVI-D_N

Fig. 4.1a shows the solution concentrations of Pb^{2+} as a function of reaction time for 1 g of nZVI-D_2, 1 g of diatomite and 0.085 g of nZVI in 500 mL of a 100 mg/L initial Pb^{2+} concentration at room temperature and the initial pH solution was adjusted to 5; the solution pH increased to 7 during the adsorption because the reaction of nZVI-D_2 and nZVI with solution were occurred. It has been resulted that 97.36% of lead ion in an aqueous solution was removed effectively by using nZVI-D_2, however 88.84% and 27.81% of lead ion were adsorbed by using nZVI and diatomite, respectively. In addition, the adsorption capability of nZVI-D_2 was 1.13 and 3.69 times greater than nZVI and diatomite, respectively.

This research was studied the initial pH at the pH of 5 since our research found that the pH of 4-6 could treat lead ions at most 94% (Arancibia-Miranda et al., 2014; X. Zhang, Lin, Chen, Megharaj, & Naidu, 2011). In case of pH < 7.0, the main species was Pb^{2+} and the removal of Pb^{2+} was mainly achieved via adsorption reaction. The adsorption of Pb^{2+} can be contributed to the ion exchange between Pb^{2+} and H^+/Si^{2+} on the surface. While the predominant species at pH 7.0-10.0 were $Pb(OH)^+$ and $Pb(OH)_2$. At pH > 10.0, the main species was $Pb(OH)_3^-$ resulting in the decrease of Pb^{2+} adsorption on nZVI-D_2 as a result of the competition between OH^- and $Pb(OH)_3^-$, and the precipitation began to form in the solution at the pH of Pb^{2+}~8.7 (Sheng et al., 2009). In addition, in this study, the pH_{pzc} values of the diatomite, and nZVI were 1.0 and 6.4, respectively, and the pH_{pzc} values of nZVI-D_N is less than 3. Since, the pH of solution was greater than pH_{pzc} of nZVI-D_N, therefore, the adsorbent surface was negative. There was an electrostatic attraction between negative-charge adsorbent surface and Pb^{2+}, which Pb^{2+} could be well adsorbed. On the other hand, the pH of solution was lower than pH_{pzc}, the charge on adsorbent surface was positive. There was an electrostatic repulsion between positive-charge adsorbent surface and Pb^{2+}, which Pb^{2+} was the lower adsorption (Irani, Amjadi, & Mousavian, 2011).

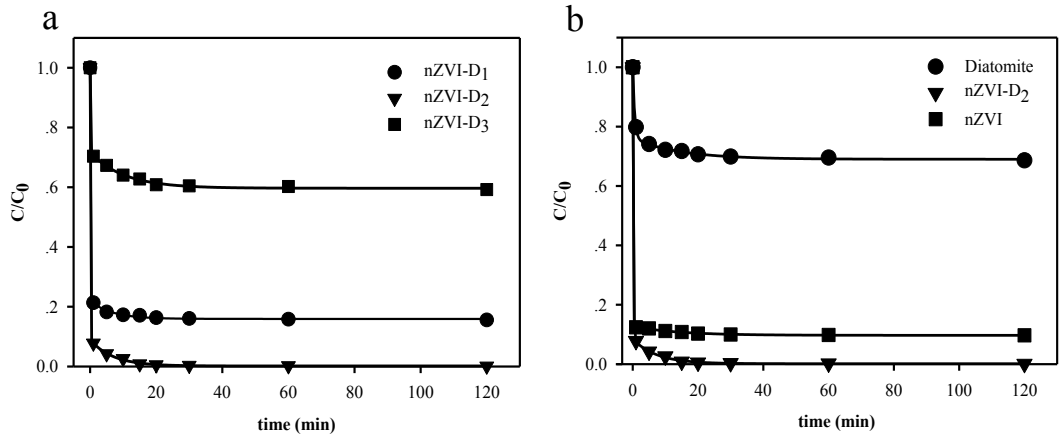

Figure 4.1 Efficiency adsorption of lead by (a) nZVI-D_1, nZVI-D_2 and nZVI-D_3 and (b) Diatomite, nZVI and nZVI-D_2 at 100 mg/L of initial lead concentration, pH 5 of initial pH and 30 ºC

The adsorption results of Pb^{2+} by Diatomite, nZVI, nZVI-D_1, nZVI-D_2 and nZVI-D_3 shown in Fig 4.1(a-b) can be conclude that the nZVI-D_2 was more effective than adsorbent other. The Fig 4.1a indicating that the coating layers of iron oxide on the diatomite affected the adsorption Pb^{2+}. That is, the double iron oxide coating on diatomite (nZVI-D_2) is effective in the treatment of Pb^{2+} up to 99.45%, followed by the nZVI-D_1 and nZVI-D_3 can be adsorbed 83.66 and 39.17%, respectively. Due to the amount of iron oxide in the double layers has dosage more than single layers one. In the case of the triple iron oxide coating has the amount of iron oxide up to 9.30% (result of chapter III) but it has been low effective in absorption Pb^{2+}. Probably due to the iron oxide was not good dispersed on the surface of diatomite and the amount of iron oxide deposits excess. As a result, the iron oxide coat on diatomite triple layers cannot reaction with $NaBH_4$ changed to nZVI-D_3 shown in Fig 4.2 of TEM images. In addition, SEM images (result of chapter III) indicated that amount of iron oxide blocked the porous structure of diatomite for the first to the double iron oxide coating and the iron oxide dispersed well in surface of diatomite. In the triple iron oxide coating, the structure of diatomite was broken to pieces and was covered by iron oxide which similar to research of Zhu, Jia, Wu, & Wang (2009).

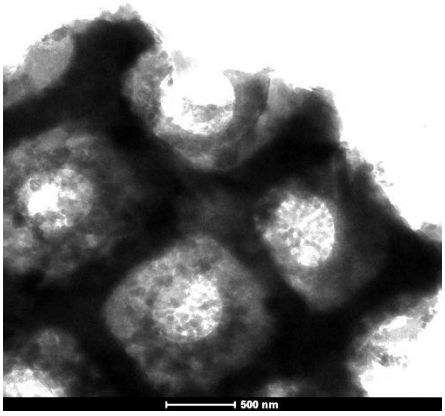

Figure 4.2 TEM images of nZVI-D_3 (triple iron oxide coating)

Fig 4.1b shows that the removal of Pb^{2+} by nZVI-D_2 has reactivity more than nZVI only and diatomite only. Therefore, the support material, diatomite helps to stabilize and disperse nZVI as well as prevent nZVI from aggregation. Whereas, diatomite can be removed Pb^{2+} about 15 %. In the case of diatomite only, absorbing occurs only for the ionic strength dependent adsorption indicating that ion exchange or outer-sphere complexation contributes to lead adsorption on diatomite at pH < 7.0 (Sheng et al., 2009). Pb^{2+} can also be adsorbed by the silanol groups (Si-OH) and alumina group (Al-OH) of diatomite. This process can be represented as (Oubagaranadin & Murthy, 2009):

$$Si\text{-}OH + Pb^{2+} \leftrightarrow Si\text{-}OPb^{+} + H^{+} \quad (4.2)$$

$$2Si\text{-}OH + Pb^{2+} \leftrightarrow (Si\text{-}O)_2Pb + 2H^{+} \quad (4.3)$$

$$Al(OH)_3 + Pb^{2+} \leftrightarrow Al(OH)\text{-}\ Pb^{2+} + 2H_2O \quad (4.4)$$

While the nZVI only, the nZVI was effective in the treatment of Pb^{2+} about 90% because nZVI acts as an active electron donator to reduce Pb^{2+} (X. Zhang et al., 2011).

$$2Fe^{0} + 3Pb_2^{+} + 4H_2O \rightarrow 3Pb^{0} + 2FeOOH + 2H^{+} \quad (4.5)$$

Therefore, it is expected that the treatment of Pb^{2+} with nZVI-D_2 was the combination of nZVI and diatomite. It was found that the occurrence of iron oxide on the surface of diatomite leaded to the adhesive bonds of Pb^{2+} and iron oxides

becoming $FeOHPb^{2+}$ complex dominantly at pH < 5.5 (Abdel-Samad & Watson, 1998).

4.4.2 Adsorption isotherm

Adsorption isotherms were significant for reporting how molecules or ions of adsorbate interact with adsorbent surface sites. Three isotherm equations, namely, Langmuir, Freundlich and, Dubinin-Radushkevich were tested which could be shown by the following equation:

$$\frac{C_e}{q_e} = \frac{C_e}{q_m} + \frac{1}{q_m K_L} \tag{2.3}$$

$$\log q_e = \log k_F + \frac{1}{n} \log C_e \tag{2.5}$$

$$\ln q_e = \ln q_d - \beta \varepsilon^2 \tag{2.6}$$

The Langmuir adsorption isotherms was determined the maximum adsorption capacity as 158.73 mg/g. Similar observation was reported by the adsorption of lead on raw bentonite, iron-coated bentonite and magnesium-coated bentonite, bentonite, kaolin and active carbon (Mishra, & Patel, 2009) and untreated diatomite and Mn-diatomite (Khraisheh, Al-degs, & Mcminn, 2004). In our case, the R_L value is 0.0018-0.0096, and it is confirmed that the preparedness nZVI-D_2 prefer adsorption of lead ions for the initial concentration of 250-1,250 mg/L. Therefore, the adsorption process is favorable. In addition, Freundlich isotherm equation is shown the value of Freundlich constants (n) which is equal to 11.123 meaning chemisorptions process. It shows that there were a strong absorption between the adsorbate and adsorbent. Moreover, The Dubinin–Radushkevich (D–R) adsorption isotherm model predicts the energy of adsorption per unit of adsorbate. Then, the adsorption energy (E) in this research is 54.78 kJ/mol which defining the type of adsorption of Pb^{2+} on nZVI-D_2 as chemical adsorption (Caliskan, Kul, Alkan, Sogut, & Alacabey, 2011).

So, the results of the equilibrium isotherm model and kinetic adsorption model exposed that the adsorption of Pb^{2+} on nZVI-D_2 was favored as a result of chemisorption rather than physisorption. It also indicated that the Langmuir isotherm

was better fitted to the adsorption data than the other isotherm equations shown in the Table 4.1.

Table 4.1 Adsorption isotherm parameters for lead adsorption onto nZVI-D_2

Langmuir	**value**	**Freundlich**	**value**	**Dubinin-Radushkevich**	**value**
q_e (mg/g)	158.73	n	11.12	E (kJ/mol)	54.78
K_L (L/mg)	0.488	K_F (L/g)	96.805	K_D	0.00016
R^2	0.999	R^2	0.924	R^2	0.932

Fig 4.3 shown that the result of contact time per Pb^{2+} adsorption was increased sharply in the first 5 min and reached equilibrium at 30 min which 1 g of nZVI-D_2 can be adsorb Pb^{2+} about 159 mg in 30 min. whereas, the reaction time at 5 min can be removal during Pb^{2+} about 135 mg which a similar 30 min in the condition of initial concentration of Pb^{2+} at 500-1,250 mg/L. To sum up nZVI-D_2 is capable of treatments in a quick moment.

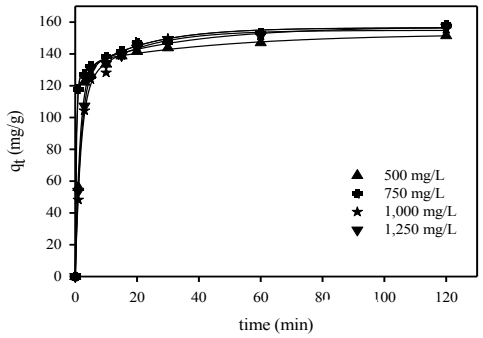

Figure 4.3 Effect of contact time per adsorption captivity on initial concentration of Pb^{2+}: 500-1,250 mg/L, 1 g of nZVI-D_2 at 30ºC

A comparison of the maximum adsorption capacity of nZVI-D_2 for Pb^{2+} with those of various adsorbents conducted within a similar concentration range is displayed in Table 4.2. The results show that the adsorption of Pb^{2+} on nZVI-D_2 was the highest, when compared with the absorption of other research.

Table 4.2 Comparisons of the maximum lead adsorption capacity onto different adsorbents

Adsorbent	Concentration range (mg/L)	Model	Adsorption Capacity (mg/g)	Reference
Expanded perlite	10-400	Langmuir	13.39	(Sari, Tuzen, Citak, & Soylak, 2007)
Iron oxide-coated bentonite	2-10	Langmuir	22.20	(Eren, 2009)
Diatomite	10-500	Freundlich	25.01	(Irani et al., 2011)
Pine cone	100	Langmuir	27.53	(Momčilović et al., 2011)
Diatomite	6-32	Freundlich	47.64	(Sheng et al., 2009)
Montmorillonite	100-200	Langmuir	52.00	(Oubagaranadin et al., 2009)
Valonia tannin resin	20-120	Langmuir	53.19	(Özacar, Şengil, & Türkmenler, 2008)
Mn-diatomite	200	Langmuir	99.00	(Al-Degs, Khraisheh, 2001)
Zero valent ion coated diatomite	250-1,250	Langmuir	158.73	This work

4.4.3 Kinetic adsorption isotherms of lead

The kinetic adsorption isotherms study can be extremely beneficial to determine the information about the mechanism of adsorption and the efficiency of the adsorbents for the removal of pollutants. In this study, the adsorption facts of lead by nZVI-D_2 were fitted by three kinetic models, including the pseudo-first-order, the pseudo-second-order and the intra-particle diffusion models, which could be shown by the following equation:

$$\log(q_e - q_t) = \log q_e - \frac{k_1}{2.303} t \quad (2.9)$$

$$\frac{t}{q_t} = \frac{1}{k_2 q_e^2} + \frac{1}{q_e} t \quad (2.10)$$

$$q_t = k_i t^{1/2}$$

(2.12)

Table 4.3 Kinetic parameters for the adsorption of lead onto nZVI-D_2 at the different concentrations

C_o (mg/L)	**500**	**750**	**1,000**	**1,250**
$q_{e,exp}$ (mg/g)	**151.44**	**155.86**	**155.56**	**156.92**
pseudo-first-order kinetic				
$q_{e,cal}$ (mg/g)	249.45	313.07	644.41	428.41
$k_1 \times 10^{-2}$ (L/min)	3.37	1.78	2.10	1.71
R^2	0.776	0.780	0.912	0.801
pseudo-second-order kinetic				
$q_{e,cal}$ (mg/g)	149.25	153.84	158.73	166.67
$k_2 \times 10^{-3}$ (g/mg·min)	5.99	5.15	3.31	4.54
R^2	0.997	0.997	0.996	0.998
intraparticle diffusion				
k_i(mmol·mg·$min^{1/2}$)	11.68	20.42	23.946	21.885
R^2	0.506	0.637	0.785	0.728

These results indicated that the adsorption of lead by nZVI-D_2 did not follow the pseudo-first-order kinetics however it well fit with the pseudo-second-order kinetic model shown in Fig 4.4(a-b). The results were found that it was similar to the adsorption of Pb^{2+} on various adsorbents reported by several authors (Mishra, & Patel, 2009; Momčilović et al., 2011). Thus indicating that chemisorption rather than physic adsorption is the rate controlling step in the adsorption process by nZVI-D_2 due to the valence forces sharing or exchanging electrons between the adsorbent and

Pb^{2+}. An increased the initial Pb^{2+} concentration from 500- 1,250 mg/L led to a decrease the pseudo-second-order rate constant (k_2) from 0.00599 to 0.00454 g/mg/min as seen in Table 4.3. This demonstrated that the reduction of Pb^{2+} occurs through a solid–liquid reaction in the interface of nZVI-D_2 and the equilibrium of contact time for the adsorption was prolonged with increasing initial Pb^{2+} concentration (Chen et al., 2013).

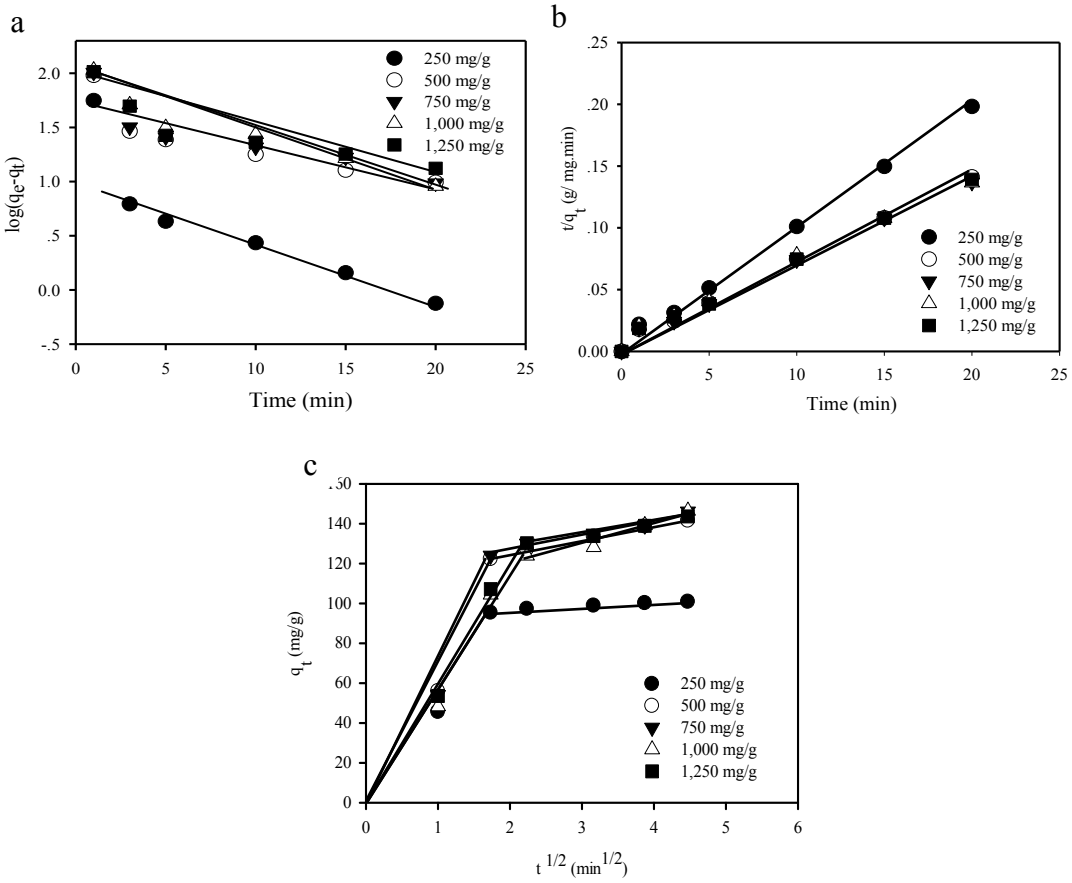

Figure 4.4 Kinetic adsorption isotherm plots (a) Pseudo-first-order kinetics Model (b) Pseudo- second-order kinetics model and (c) Intraparticle diffusion kinetics model of lead adsorption on nZVI-D_2 at 30ºC

The intra-particle diffusion found that linear was multi-linear three steps over the all-time range dominate the adsorption process. It can be concluded that the multi-linear plots were more than one process that control the rate of adsorption but only one is rate limiting. It was suggested from Fig. 4.4c that adsorption occurs in three

parts. The external surface adsorption (part 1) is completed within 5 min, then the part of intra-particle or pore diffusion is rate limiting (part 2), from 5 to 30 min. At last final equilibrium adsorption (part 3) starts after 30 min. The Pb^{2+} are slowly transported through intra-particle diffusion into the particles and is finally maintained in the micro-pores (Özacar et al., 2008), while the values of the determination coefficients (R^2) obtained from the plots of intra-particle diffusion kinetics were lower than those of the pseudo-second-order model (Table 4.3), this model indicates that the adsorption of lead ions on nZVI-D_2 may be followed by an intra-particle diffusion model up to 30 min. This suggests that the Pb-nZVI-D_2 adsorption system belongs to the second-order equation, based on the assumption that the rate-limiting step may be intra-particle diffusion, film diffusion and chemisorption involving valence forces through sharing or exchange of electrons between nZVI-D_2 and Pb^{2+}, which is similar to the absorption lead on montmorillonite-illite type clay was controlled by both intra-particle diffusion and film diffusion (Oubagaranadin, & Murthy, 2009).

All kinetic data for the adsorption of lead by nZVI-D_2, calculated from the related plots, are summarized in Table 4.3. Comparison of the R^2 values for different models suggests that the pseudo-second-order kinetics fits best due to its highest value (R^2=0.999). However, the pseudo-first-order and the intra-particle diffusion poorly fit to the experimental data for the adsorption of lead. This concluded that the nZVI-D_2-Pb adsorption system is the second-order kinetics; based on the assumption that the rate limiting step may be chemisorption involving valence forces through exchange of electrons between nZVI-D_2 and Pb^{2+}.

The adsorption isotherm and kinetic absorption can be confirmed that mass transfer and intraparticle diffusion were the rate-limiting steps together. The first phase of the ion exchange of $Pb^{2+}$from nZVI-D_2 aqueous solution with nZVI and the second part was caused by the diffusion of Pb^{2+} into the interior. It is found that the absorption in the second part of the chemisorption, which involved valence forces through exchange of electrons between nZVI-D_2 and Pb^{2+}. In short, the adsorption Pb^{2+} with nZVI-D_2 was predicted Langmuir isotherms model and the pseudo-second-order kinetics model, which shown that the mechanism of Pb^{2+} adsorption was chemisorption.

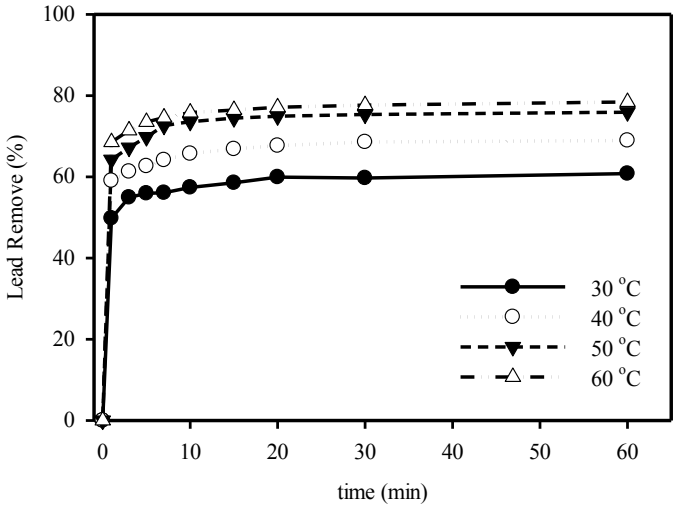

Figure 4.5 Effect of temperature on the adsorption thermodynamic of Pb^{2+} by nZVI-D_2 at 400 mg/L: initial concentration, 1 g/L: nZVI-D_2 and pH 5

The thermodynamic parameters obtained are shown in Table 4.4. An increase of temperature resulted in an increasing rate of lead adsorption indicating that the process is endothermic (Fig. 4.5). A similar trend has been reported for the removal of cadmium by nano zero-valent iron particles (Boparai, Joseph, & O'Carroll, 2011). Negative values of ΔG^O indicate that spontaneous adsorption and the degree of spontaneity of the reaction increases with increasing temperatures. It is clear that the free energy of lead adsorption on nZVI-D_2 is more negative at higher temperatures, which demonstrates that the spontaneity of the adsorption process increases with the rise in temperature. The ΔH^O values were in the range of 15.26-47.11 kJ/mol with a mean value of 23.97 kJ/mol. The values conform to the endothermic nature of the adsorption process. The positive values of ΔS^O were in the range of 61.00-155.37 J/mol.K with a mean value of 87.30 J/mol K. The positive value of ΔS° suggests that the structural changes occur on the adsorbent and the unstructured at the solid/liquid interface in the adsorption system increases during the adsorption process which is similar to the research of Sheng et al. (Kul & Koyuncu, 2010) who studied the temperature-dependent adsorption of Pb^{2+} on diatomite. The results indicated that the adsorption process of Pb^{2+} on nZVI-D_2 was spontaneous and endothermic in nature.

Table 4.4 Values of thermodynamic parameters for the lead adsorption onto nZVI-D_2

C_o	ΔH^o	ΔS^o	ΔG^o(kJ/mol)			
(mg/L)	(kJ/mol)	(J/mol K)	30ºC	40ºC	50ºC	60ºC
300	16.34	68.38	-4.38	-5.06	-5.74	-6.43
400	15.26	61.44	-3.35	-3.97	-4.58	-5.19
500	17.15	64.00	-2.25	-2.88	-3.52	-4.16
600	47.11	155.37	-0.010	-1.54	-3.09	-4.65

4.4.4 Mechanism of lead adsorption on nZVI-D

The XPS analysis results were found that elementary elements in the nZVI-D_2 were at Fe 2p 709.1 eV, O 1s 530.1 eV, C 1s 283.1 eV, Si 2p 101.1 eV and Al 2p 73.1 eV as shown in Fig 4.6a. The peaks at 705.3 eV corresponding to zero-valent iron (Fe^0 $2p_{3/2}$), while 711.5 eV and 725.2 eV corresponded to Fe $2p_{3/2}$ and Fe $2p_{1/2}$ binding energies, the main iron species of nZVI-D_2 were Fe^0, Fe_2O_3 ,$Fe(OH)_3$ and FeOOH (Hermas, 2008) is given in Fig 4.6b. It was confirmed that the outer shell structure of nZVI-D presented iron oxides and iron hydroxide consistent with research of Zhang et al. (2011) Through, the binding energy analyzes, Si 2p peaks at 101.7 eV and 102.8 eV were assigned to the Si-O and Si-OH, respectively while the Al 2p peak at 73.4 eV and 74.6 eV was AlOOH and Al(OH), respectively.

After adsorption Pb^{2+} the peak corresponding to Fe^0 was not observed, while the XPS spectra showed Fe_2O_3, FeO and FeOOH as the dominant energy peak. This result indicated that Fe^0 can be severely oxidized to Fe_2O_3, FeO and FeOOH as shown in Fig 4.6c. Moreover, the data was found that SiO_2 and $Al(OH)_3$ after adsorption, which possible that the oxidation of Si-O, Si-OH, AlOOH and $Al(OH)_3$ respectively. At the same time, The Pb $4f_{7/2}$ and Pb $4f_{5/2}$ narrow scans were illustrated in Fig 4.6d. The spectra have positioned at 138.9 and 143.7 eV, which is dispersed to $Pb(OH)_2$ and PbO, respectively (Özlem Kocabaş-Ataklı, & Yürüm, 2013; Zhang et al., 2011). Nevertheless, Pb^0 was not detected on the XPS data, but the XRD analysis confirmed the existence of Pb^0 (An, Zhao, Jia, Wu, & Wang, 2009; Gil, Carbonio, & Gómez, 2010; Laurindo, Bocchi, & Rocha-Filho, 2000; Zhang &

Houlachi, 2010) (Fig 4.7). Indicating that Pb^0 may be adsorbed into the core structure of Fe^0, which may be more deep from the surface than the detection limitation of XPS analysis (Woo, Park, Lee, & Lee, 2014) In this interesting note that, the peaks ratio of the oxygen at 531.5 and 532.3 eV (Fig 4.6e) increased after Pb^{2+} adsorption, suggesting that hydroxyl bonded to metal groups (M-OH) and metal oxide groups (M-O) (Artyushkova, Levendosky, Atanassov, & Fulghum, 2007; Mekki, Holland, McConville, & Salim, 1996) build on the surface of nZVI-D_2 which confirmed that the Pb^{2+} adsorbed on the surface of nZVI-D_2 in the form of $Pb(OH)_2$ and PbO. In could be summarized that the nZVI-D_2 adsorbed Pb^{2+} has been observed the Pb^0, $Pb(OH)_2$, PbO on the surface of nZVI-D_2.

The study mechanisms of Pb^{2+} adsorption on nZVI-D_2 were mainly depended on the type of active sites on the surface of adsorbent and species of adsorbate at pH value. In this study examined the initial solution at pH 5 which the predominate specie of lead ion was mainly Pb^{2+} in solution. Based upon the more premise discussed above, a species of iron oxide, lead iron, surface of diatomite for Pb^{2+} removal on the nZVI-D_2 is presented in Fig 4.6 and 4.7. It can be suggested the mechanisms of the Pb^{2+}-nZVI-D_2 reaction which can divide into three sections.

Section I: the Fe^0 is oxides by water and oxygen, which is a natural corrosion reaction, to form Fe_2O_3 and FeOOH explained by Eq. 4.7-4.8. Then the Pb^{2+} is reduced to Pb^0 by electrons donated from Fe^0 oxidations due to the standard reduction potential of Pb^{2+}/Pb^0 is -0.1263 V which is greater than that of Fe^{2+}/Fe^0 (-0.4402 V) (Xi, Mallavarapu, & Naidu, 2010) illuminated by Eq. 4.9-4.10 and Fig 4.8 (Reaction process).

$$Fe^0 + 2H_2O \rightarrow Fe^{2+} + H_2 + 2OH^- \quad (4.7)$$

$$2Fe^0 + 2H_2O + O_2 \rightarrow Fe^{2+} + 4OH^- \quad (4.8)$$

$$2Fe^{2+} + H_2O + 0.5O_2 \rightarrow 2Fe^{3+} + 2OH^- \quad (4.9)$$

$$Fe^0 + Pb^{2+} + H_2O/O_2 \rightarrow Fe^{2+}/Fe^{3+} + Pb^0 + H_2 \quad (4.10)$$

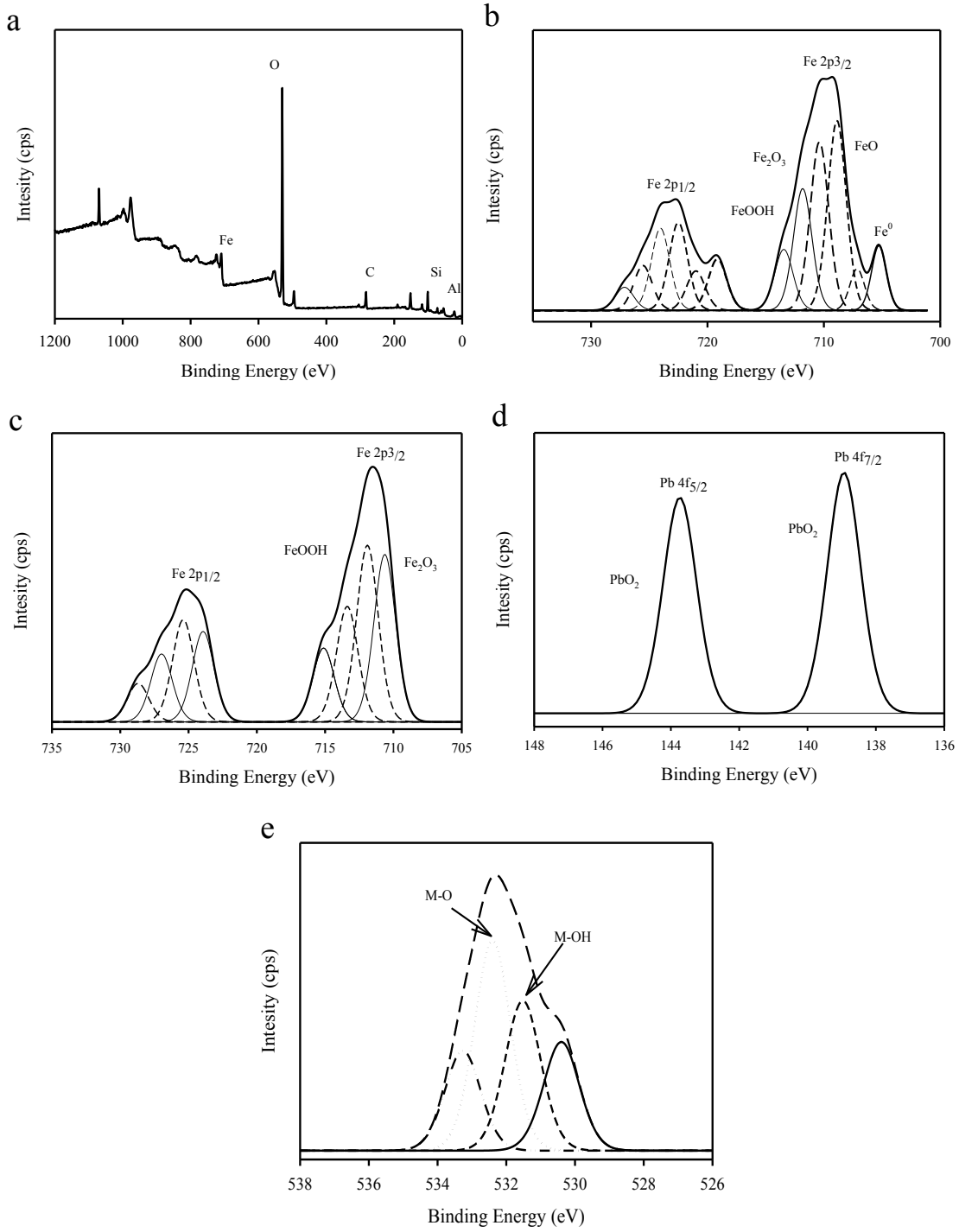

Figure 4.6 XPS spectra of (a) full survey of nZVI-D_2 before adsorption (b) iron in nZVI-D_2 before adsorption (c) iron in nZVI-D_2 after adsorption (d) lead in nZVI-D_2 after adsorption and (e) oxygen in nZVI-D_2 after adsorption at 1 mg/L of lead, 60 min

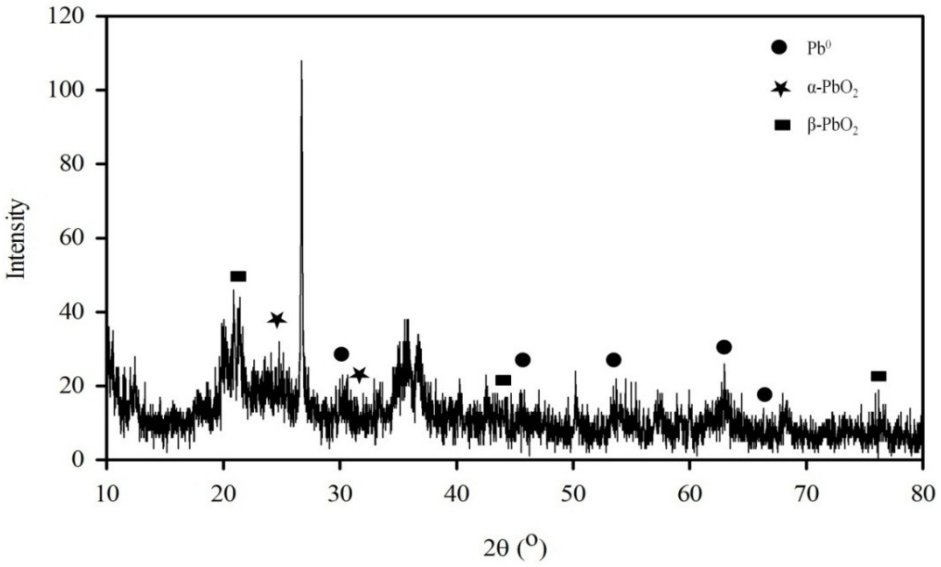

Figure 4.7 XRD pattern of nZVI-D_2 reacting with 1 mg/L of lead at 60 min

Section II: The Fe_2O_3, FeOH and FeOOH on the surface nZVI-D_2 of can react with the Pb^{2+} to produce FeOPbOH, PbO-Fe, PbO_2-Fe_2O_3 and PbO-FeOOH (pathway 1-4) which proposed by Eq. 4.11-4.14 and Fig. 4.8 (metal oxide formation for iron oxide with Pb^{2+} 1-4).

$$Fe(OH)_3 + Pb^{2+} + H_2O \rightarrow FeOPbOH + H^+ \quad (4.11)$$

$$FeOH + Pb^{2+} \rightarrow Fe\text{-}PbO + H^+ \quad (4.12)$$

$$Fe\text{-}PbO + H_2O \rightarrow FeOOH\text{-}Pb + H^+ \quad (4.13)$$

$$Fe_2O_3 + Pb^{2+} + H_2O \rightarrow Fe_2O_3\text{-}PbO + 2H^+ \quad (4.14)$$

Section III: Pb^{2+} was electron exchanged and adsorbed on the surface of diatomite which has Si-OH and Si-O to form the PbO_2-Si and PbO-Si, respectively (pathway 5-6) and Pb^{2+} can be adsorbed by the AlOOH and $Al(OH)_3$ in the diatomite structure to form $Pb(OH)_2$-Al and PbO_2-Al_2O_3 which suggested by Eq. 4.15-4.18 and Fig. 4.8 (metal oxide formation for silica oxide and alumina oxide with Pb^{2+} 5-8).

$$Si\text{-}OH + Pb^{2+} \rightarrow PbO_2\text{-}Si + 2H^+ \quad (4.15)$$

$$Si\text{-}O + Pb^{2+} \rightarrow PbO\text{-}Si + H^+ \quad (4.16)$$

$$AlOOH + Pb^{2+} \rightarrow Pb(OH)_2\text{-}Al + 2H^+ \quad (4.17)$$

$$Al(OH)_3 + Pb^{2+} \rightarrow PbO_2\text{-}Al_2O_3 + 3H^+ \quad (4.18)$$

In summary, the removal mechanism of Pb^{2+} on nZVI-D_2 was proposed all three stages including (i) Pb^{2+} changed to Pb^0 with oxidation of nZVI (ii) ferrous ions reacted with the Pb^{2+} turning to FeOPbOH, PbO-Fe, PbO_2-Fe_2O_3 and PbO-FeOOH and (iii) Pb^{2+} turned to the PbO_2-Si, PbO-Si, $Pb(OH)_2$-Al and PbO_2-Al_2O_3 on the surface of diatomite.

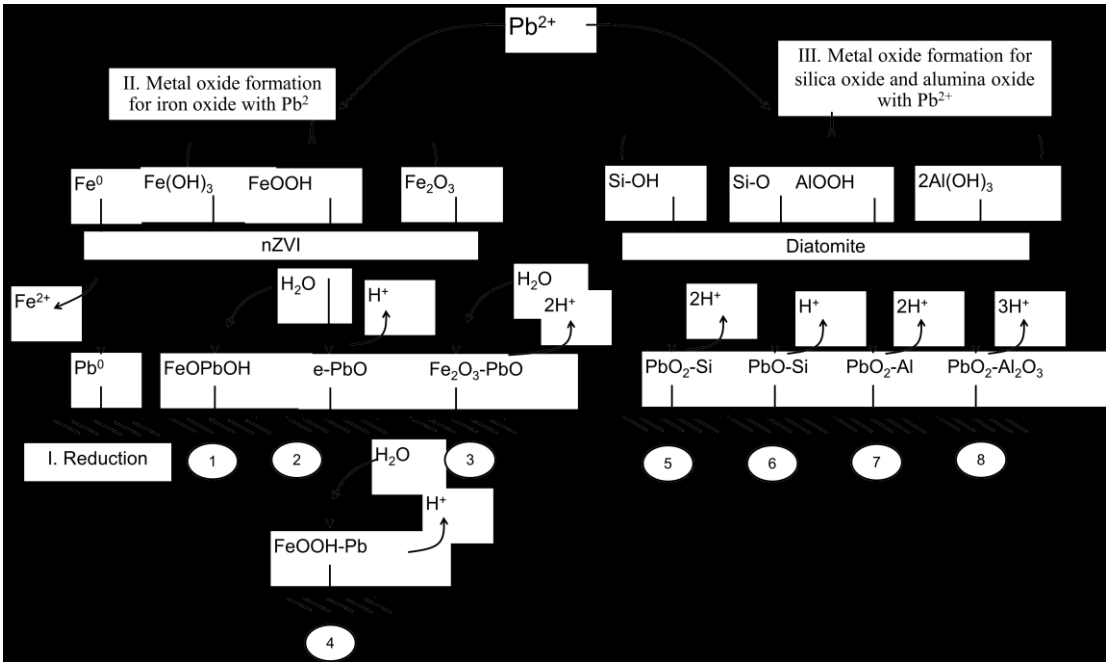

Figure 4.8 The mechanism of adsorption lead from aqueous solution by nZVI-D_2

4.5 Conclusions

The nanosized zero-valent iron (nZVI) particles were success-fully loaded onto diatomite by reduction method. The results of in this research apparently, the removal percentage of Pb^{2+} by nZVI-D_2 was higher than diatomite, nZVI, nZVI-D_1 and nZVI-D_3. The Langmuir isotherm showed a better fit than the Freundlich isotherm, thus, indicating the applicability of monolayer coverage. The mean adsorption energy was shown 54.78 kJ/mol of D-R isotherm indicating that the adsorption of Pb^{2+} on nZVI-D_2 was chemical adsorption. Furthermore, the good fit of the pseudo-second-order kinetics for adsorption in the adsorption-reduction process described the adsorption as

a chemical interaction process involving valence forces. In addition, the intra-particle diffusion was involved in the adsorption process but intra-particle diffusion was not the only rate-controlling step. Moreover, the thermodynamic parameters indicated the adsorption was an endothermic process occurring on nZVI-D_2 surface.

For the mechanism of nZVI-D_2 to remove Pb^{2+} included reaction process, ions attraction, solid-phase redox transformation and adsorptions which was proposed that, (i) Pb^{2+} were oxidized to Pb^0 on nZVI active sites, (ii) ferrous ions reacted with the Pb^{2+} to form FeOPbOH, PbO-Fe, PbO_2-Fe_2O_3, and PbO-FeOOH species on nZVI surface, and (iii) Pb^{2+} turned to PbO_2-Si, PbO-Si, $Pb(OH)_2$-Al, and PbO_2-Al_2O_3 on diatomite surface. It is concluded that nZVI-D_2 was the best efficient to use as adsorbents, which are low cost and easy synthesis suitable for the treatment of Pb^{2+} in solution.

4.6 List of abbreviations

Y	percentages lead removal
ΔG^o	gibbs free energy change
ΔH^o	enthalpy change
ΔS^o	entropy change
C_e	equilibrium concentrations solution (mg/L)
C_o	initial solution concentrations (mg/L)
C_t	concentration solution at time (mg/L)
E	mean adsorption energy (kJ/mol)
k_1	rate constant of pseudo-first-order adsorption (min^{-1})
k_2	rate constant of pseudo-second-order adsorption (g/mg·min)
k_i	intra-particle diffusion rate constant (mmol/g·$min^{1/2}$)
K_D	Dubinin-Radushkevich constant
K_F	Freundlich adsorption constant (L/g)
K_L	Langmuir adsorption constant (L/mg)
M	mass of adsorbent (g)
n	Freundlich constants
q_e	adsorption capacity at equilibrium (mg/g)

$q_{e.exp}$	adsorption capacity at equilibrium from experimental data(mg/g)
$q_{e,cal}$	adsorption capacity at equilibrium from calculated equation (mg/g)
R^2	determination coefficients
R_L	dimensionless separation factor of Langmuir adsorption
t	time (min)
V	volume of the solution (L)

4.7 References

Abdel-Samad, H., & Watson, P.R. (1998). An XPS study of the adsorption of lead on goethite (α-FeOOH). **Applied Surface Science, 136**(1-2), 46–54.

Al-Degs, Y., Khraisheh, M.A., & Tutunji, M.F. (2001). Sorption of lead ions on diatomite and manganese oxides modified diatomite. **Water Research, 35**(15), 3724–3728.

An, H., Zhao, X., Jia, Z., Wu, C., & Wang, Y. (2009). Synthesis of magnetic Pb/Fe3O4/SiO2 and its catalytic activity for propylene carbonate synthesis via urea and 1,2-propylene glycol. **Frontiers of Chemical Engineering in China, 3**(2), 215–218.

Arancibia-Miranda, N., Baltazar, S.E., García, A., Romero, A.H., Rubio, M.A., & Altbir, D. (2014). Lead removal by nano-scale zero valent iron: Surface analysis and pH effect. **Materials Research Bulletin, 59,** 341–348.

Artyushkova, K., Levendosky, S., Atanassov, P., & Fulghum, J. (2007). XPS Structural Studies of Nano-composite Non-platinum Electrocatalysts for Polymer Electrolyte Fuel Cells. **Topics in Catalysis, 46**(3-4), 263–275.

Bessbousse, H., Rhlalou, T., Verchère, J.F., & Lebrun, L. (2008). Removal of heavy metal ions from aqueous solutions by filtration with a novel complexing membrane containing poly(ethyleneimine) in a poly(vinyl alcohol) matrix. **Journal of Membrane Science, 307**(2), 249–259.

Boparai, H.K., Joseph, M., & O'Carroll, D.M. (2011). Kinetics and thermodynamics of cadmium ion removal by adsorption onto nano zerovalent iron particles. **Journal of Hazardous Materials, 186**(1), 458–465.

Caliskan, N., Kul, A.R., Alkan, S., Sogut, E.G., & Alacabey, İ. (2011). Adsorption of Zinc(II) on diatomite and manganese-oxide-modified diatomite: A kinetic and equilibrium study. **Journal of Hazardous Materials, 193,** 27–36.

Chao, H.P., & Chang, C.C. (2012). Adsorption of copper(II), cadmium(II), nickel(II) and lead(II) from aqueous solution using biosorbents. **Adsorption, 18**(5-6), 395–401.

Chen, Z., Wang, T., Jin, X., Chen, Z., Megharaj, M., & Naidu, R. (2013). Multifunctional kaolinite-supported nanoscale zero-valent iron used for the adsorption and degradation of crystal violet in aqueous solution. **Journal of Colloid and Interface Science, 398,** 59–66.

Dou, C., & Zhang, J. (2011). Effects of lead on neurogenesis during zebrafish embryonic brain development. **Journal of Hazardous Materials, 194,** 277–282.

Dou, X., Li, R., Zhao, B., & Liang, W. (2010). Arsenate removal from water by zero-valent iron/activated carbon galvanic couples. **Journal of Hazardous Materials, 182**(1-3), 108–114.

Eren, E. (2009). Removal of lead ions by Unye (Turkey) bentonite in iron and magnesium oxide-coated forms. **Journal of Hazardous Materials, 165**(1–3), 63–70.

Feng, Q., Lin, Q., Gong, F., Sugita, S., & Shoya, M. (2004). Adsorption of lead and mercury by rice husk ash. **Journal of Colloid and Interface Science, 278**(1), 1–8.

Gil, D.M., Carbonio, R.E., & Gómez, M.I. (2010). Synthesis of $Pb_2Fe_2O_5$ by thermak decomposition of $Pb_2[Fe(CN)_6].4H_2O$. **Journal of the Chilean Chemical Society, 55**(2), 189–192.

Hermas, A.A. (2008). XPS analysis of the passive film formed on austenitic stainless steel coated with conductive polymer. **Corrosion Science, 50**(9), 2498–2505.

Irani, M., Amjadi, M., & Mousavian, M.A. (2011). Comparative study of lead sorption onto natural perlite, dolomite and diatomite. **Chemical Engineering Journal, 178,** 317–323.

Khraisheh, M.A.M., Al-degs, Y.S., & Mcminn, W.A.M. (2004). Remediation of wastewater containing heavy metals using raw and modified diatomite. **Chemical Engineering Journal, 99**(2), 177–184.

Kim, S.A., Kamala-Kannan, S., Lee, K.J., Park, Y.J., Shea, P.J., Lee, W.H. et al. (2013). Removal of Pb(II) from aqueous solution by a zeolite–nanoscale zero-valent iron composite. **Chemical Engineering Journal, 217,** 54–60.

Köseoglu, R., Köksal, F., Çiftci, E., & Akkurt, M. (2005). Identification of paramagnetic radicals in γ-irradiated natural diatomite minerals by electron paramagnetic resonance. **Journal of Molecular Structure, 733**(1–3), 151–154.

Kul, A.R., & Koyuncu, H. (2010). Adsorption of Pb(II) ions from aqueous solution by native and activated bentonite: kinetic, equilibrium and thermodynamic study. **Journal of Hazardous Materials, 179**(1-3), 332–339.

Kundu, S., & Gupta, A.K. (2007). Adsorption characteristics of As(III) from aqueous solution on iron oxide coated cement (IOCC). **Journal of Hazardous Materials, 142**(1–2), 97–104.

Laurindo, E.A., Bocchi, N., & Rocha-Filho, R.C. (2000). Production and characterization of TI/PbO2 electrodes by a thermal-electrochemical method. **Journal of the Brazilian Chemical Society, 11**(4), 429–433.

Li, X., Elliott, D.W., & Zhang, W. (2006). Zero-Valent Iron Nanoparticles for Abatement of Environmental Pollutants: Materials and Engineering Aspects. **Critical Reviews in Solid State and Materials Sciences, 31**(4), 111–122.

Mak, M.S.H., Rao, P., & Lo, I.M.C. (2011). Zero-valent iron and iron oxide-coated sand as a combination for removal of co-present chromate and arsenate from groundwater with humic acid. **Environmental Pollution (Barking, Essex: 1987), 159**(2), 377–382.

Mekki, A., Holland, D., McConville, C.F., & Salim, M. (1996). An XPS study of iron sodium silicate glass surfaces. **Journal of Non-Crystalline Solids, 208**(3), 267–276.

Mishra, P.C., & Patel, R.K. (2009). Removal of lead and zinc ions from water by low cost adsorbents. **Journal of Hazardous Materials, 168**(1), 319–325.

Momčilović, M., Purenović, M., Bojić, A., Zarubica, A., & Ranđelović, M. (2011). Removal of lead(II) ions from aqueous solutions by adsorption onto pine cone activated carbon. **Desalination, 276**(1–3), 53–59.

Naeem, A., Saddique, M.T., Mustafa, S., Kim, Y., & Dilara, B. (2009). Cation exchange removal of Pb from aqueous solution by sorption onto NiO. **Journal of Hazardous Materials, 168**(1), 364–368.

Oubagaranadin, J.U.K., & Murthy, Z.V.P. (2009). Adsorption of Divalent Lead on a Montmorillonite−Illite Type of Clay. **Industrial & Engineering Chemistry Research, 48**(23), 10627–10636.

Özacar, M., Şengil, İ.A., & Türkmenler, H. (2008). Equilibrium and kinetic data, and adsorption mechanism for adsorption of lead onto valonia tannin resin. **Chemical Engineering Journal, 143**(1–3), 32–42.

Özlem Kocabaş-Ataklı, Z., & Yürüm, Y. (2013). Synthesis and characterization of anatase nanoadsorbent and application in removal of lead, copper and arsenic from water. **Chemical Engineering Journal, 225,** 625–635.

Pan, Y.F., Chiou, C.T., & Lin, T.F. (2010). Adsorption of arsenic(V) by iron-oxide-coated diatomite (IOCD). **Environmental Science and Pollution Research International, 17**(8), 1401–1410.

Ponder, S.M., Darab, J.G., Bucher, J., Caulder, D., Craig, I., Davis, L. et al. (2001). Surface chemistry and electrochemistry of supported zerovalent iron nanoparticles in the remediation of aqueous metal contaminants. **Chemistry of Materials, 13**(2), 479–486.

Sari, A., Tuzen, M., Citak, D., & Soylak, M. (2007). Adsorption characteristics of Cu(II) and Pb(II) onto expanded perlite from aqueous solution. **Journal of Hazardous Materials, 148**(1-2), 387–394.

Schmitt, C.J., Brumbaugh, W.G., & May, T.W. (2007). Accumulation of metals in fish from lead–zinc mining areas of southeastern Missouri, USA. **Ecotoxicology and Environmental Safety, 67**(1), 14–30.

Sheng, G., Wang, S., Hu, J., Lu, Y., Li, J., Dong, Y., & Wang, X. (2009). Adsorption of Pb(II) on diatomite as affected via aqueous solution chemistry and temperature. **Colloids and Surfaces A: Physicochemical and Engineering Aspects, 339**(1–3), 159–166.

WHO. (2012). **WHO Guidelines for drinking-water quality.** Retrieved November 10, 2012, from http://www.who.int/water_sanitation_health/dwq/guidelines/en/

Woo, H., Park, J., Lee, S., & Lee, S. (2014). Effects of washing solution and drying condition on reactivity of nano-scale zero valent irons (nZVIs) synthesized by borohydride reduction. **Chemosphere, 97,** 146–152.

Xi, Y., Mallavarapu, M., & Naidu, R. (2010). Reduction and adsorption of Pb^{2+} in aqueous solution by nano-zero-valent iron—A SEM, TEM and XPS study. **Materials Research Bulletin, 45**(10), 1361–1367.

Zhang, W., & Houlachi, G. (2010). Electrochemical studies of the performance of different Pb–Ag anodes during and after zinc electrowinning. **Hydrometallurgy, 104**(2), 129–135.

Zhang, X., Lin, S., Chen, Z., Megharaj, M., & Naidu, R. (2011). Kaolinite-supported nanoscale zero-valent iron for removal of Pb^{2+} from aqueous solution: reactivity, characterization and mechanism. **Water Research, 45**(11), 3481–3488.

Zhang, X., Lin, S., Lu, X.Q., & Chen, Z. (2010). Removal of Pb(II) from water using synthesized kaolin supported nanoscale zero-valent iron. **Chemical Engineering Journal, 163**(3), 243–248.

Zhang, Y., Li, Y., Li, J., Hu, L., & Zheng, X. (2011). Enhanced removal of nitrate by a novel composite: Nanoscale zero valent iron supported on pillared clay. **Chemical Engineering Journal, 171**(2), 526–531.

Zhu, H., Jia, Y., Wu, X., & Wang, H. (2009). Removal of arsenic from water by supported nano zero-valent iron on activated carbon. **Journal of Hazardous Materials, 172**(2–3), 1591–1596.